Computational Analyses in Support of Sub-scale Diffuser Testing for the A-3 Facility – Part 2: Unsteady Analyses and Risk Assessment

Vineet Ahuja[1] and Ashvin Hosangadi[2]
Combustion Research and Flow Technology, Pipersville, PA 18947

and

Daniel Allgood[3]
NASA Stennis Space Center, MS 39529, USA

Simulation technology can play an important role in rocket engine test facility design and development by assessing risks, providing analysis of dynamic pressure and thermal loads, identifying failure modes and predicting anomalous behavior of critical systems. This is especially true for facilities such as the proposed A-3 facility at NASA SSC because of a challenging operating envelope linked to variable throttle conditions at relatively low chamber pressures. Design Support of the feasibility of operating conditions and procedures is critical in such cases due to the possibility of startup/shutdown transients, moving shock structures, unsteady shock-boundary layer interactions and engine and diffuser unstart modes that can result in catastrophic failure. Analyses of such systems is difficult due to resolution requirements needed to accurately capture moving shock structures, shock-boundary layer interactions, two-phase flow regimes and engine unstart modes. In a companion paper, we will demonstrate with the use of CFD, steady analyses advanced capability to evaluate supersonic diffuser and steam ejector performance in the sub-scale A-3 facility. In this paper we will address transient issues with the operation of the facility especially at startup and shutdown, and assess risks related to afterburning due to the interaction of a fuel rich plume with oxygen that is a by-product of the steam ejectors. The primary areas that will be addressed in this paper are: (1) analyses of unstart modes due to flow transients especially during startup/ignition, (2) engine safety during the shutdown process (3) interaction of steam ejectors with the primary plume i.e. flow transients as well as probability of afterburning. *In this abstract we discuss unsteady analyses of the engine shutdown process. However, the final paper will include analyses of a staged startup, drawdown of the engine test cell pressure, and risk assessment of potential afterburning in the facility.*

Unsteady simulations have been carried out to study the engine shutdown process in the facility and understand the physics behind the interactions between the steam ejectors, the test cell and the supersonic diffuser. As a first approximation, to understand the dominant unsteady mechanisms in the engine test cell and the supersonic diffuser, the turning duct in the facility was removed. As the engine loses power a rarefaction wave travels downstream that disrupts the shock cell structure in the supersonic diffuser. Flow from the test cell is seen to expand into the supersonic diffuser section and re-pressurizes the area around the nozzle along with a upstream traveling compression wave that emanates from near the first stage ejectors. Flow from the first stage ejector expands to the center of the duct and a new shock train is formed between the first and second stage ejectors. Both stage ejectors keep the facility pressurized and prevent any large amplitude pressure fluctuations from affecting the engine nozzle. The resultant pressure loads the nozzle experiences in the shutdown process are small.

Details of the unsteady shutdown simulation are shown in Figure 1. The shutdown process is initiated by turning the mass flow from the engine nozzle inflow boundary off impulsively. The pressure at the boundary is computed from solving the momentum conservation equations and does not instantaneously drop. Rather it drops from a driving pressure of 1337 psia to 0.16 psia in 12.89 milli-seconds. The evolution of the flow is shown in Figure 1 where a series of snapshots of Mach number distribution in the facility are shown. As the engine loses power, and consequently the pressure drops inside and at the exit plane of the nozzle the strong under-expanded jet through the nozzle exit, weakens turns parallel to the jet axis (0.00684 secs). This triggers an expansion wave that travels downstream through the supersonic diffuser section. As the expansion wave travels downstream, the strong pressure

[1] Senior Research Scientist, 6210 Keller's Church Rd., and AIAA Senior Member.
[2] Principal Scientist, 6210 Keller's Church Rd., and AIAA Senior Member.
[3] Aerospace Engineer, Stennis Space Center, MS 39529-6000, and AIAA Member.

gradient between the test chamber and the section of the supersonic diffuser close to the nozzle exit drives the flow from the test chamber into the supersonic diffuser towards the central axis. The flow entrainment from the test cell re-pressurizes the supersonic diffuser section just downstream of the nozzle exit and a small amount of backflow enters the nozzle.

As the rarefaction wave travels downstream near the plane of the first stage steam ejector it changes the shock cell structure in the duct between the first stage and second stage steam ejectors. As the incoming flow Mach number weakens, it changes the deviation angle of the shock cell that gives the impression that the shock cell structure is moving upstream as it is weakening. Flow from the first stage ejectors expands towards the centerline and forms a new shock train in the duct between the first and second stage ejectors. Furthermore a compression wave is seen traveling upstream from the first stage ejector plane towards the engine nozzle. This compression wave first interacts with the expansion wave formed near the corner of the supersonic diffuser where the area contraction straightens out. Moving upstream it then interacts with the oblique shock near the diffuser wall where the diffuser area contracts. Finally it interacts with the flow expansion between the test cell and the supersonic diffuser near the exit plane of the nozzle and remnants of flow from the nozzle forming multiple reflections and a complex flow pattern that includes a triple point.

Meanwhile, as the flow in the duct between the first and second stage ejectors settles into a new shock train pattern, the pressurization across the plane of the second stage ejector changes near the centerline in the core flow. As a consequence, the oblique shock near the centerline close to the plane of the second stage ejector steepens till it turns into a normal shock. Thus the shock train in the duct between the first stage and second stage ejectors transitions into a normal shock by the second stage ejectors. More importantly, the flow in the facility past the first stage ejector plane remains supersonic throughout the shutdown process.

Figure 2 shows the line plot of the pressure distribution along the centerline matched against the location and pressure distribution in the facility. As a result, the pressure in the nozzle, expansion of the engine plume, shock train structure, and pressure drop in exit diffuser can be clearly seen and compared to the physical locations in the facility. The line plots (Figure 2 and 3) are plotted in a log scale to accommodate the large variation in pressure between the nozzle at full power to the low pressures seen near the nozzle after shutdown. The line plots in Figure 3 clearly show the pressure dropping in the engine and the downstream traveling rarefaction wave indicated by the weakening (smaller amplitudes) of the oblique shocks in the diffuser section just aft of the nozzle. Furthermore, we also see the weakening of the shock cell structure in the duct between the first and second stage ejectors and the reformation of a new shock cell structure in the duct as the flow from the first stage ejector expands out. The formation and eventual migration of the upstream traveling compression wave from the first stage ejectors can also be seen as the centerline pressure in the supersonic diffuser rises, as is the transition of the oblique shock near the second stage ejectors to a normal shock. Both the first and second stage ejectors are seen to pressurize the duct and maintain fairly constant pressure levels. As a result, the pressure distribution in the exit diffuser does not change much during the shutdown process. This is indicative of the fact that both the ejector stages are performing satisfactorily and prevent any blow-back or large scale pressure fluctuations from entering the engine. Lastly, the pressure loading in and around the nozzle after shutdown is fairly small and average pressures range between 100-200 Pa (0.015-0.029 psia) as seen in the centerline pressure plots.

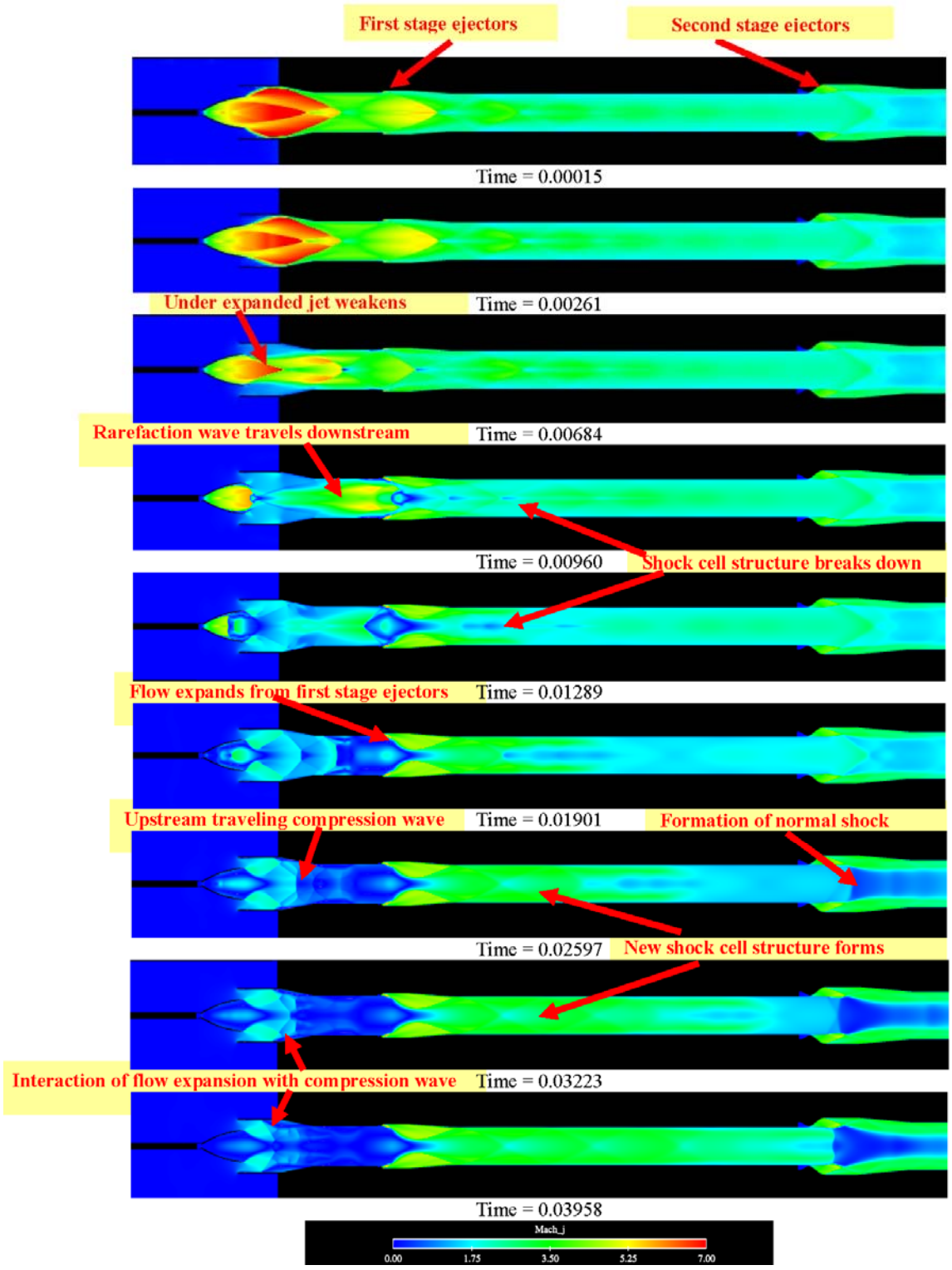

Figure 1. Sequence of Mach Number distributions showing evolution of flow in the facility during engine shutdown.

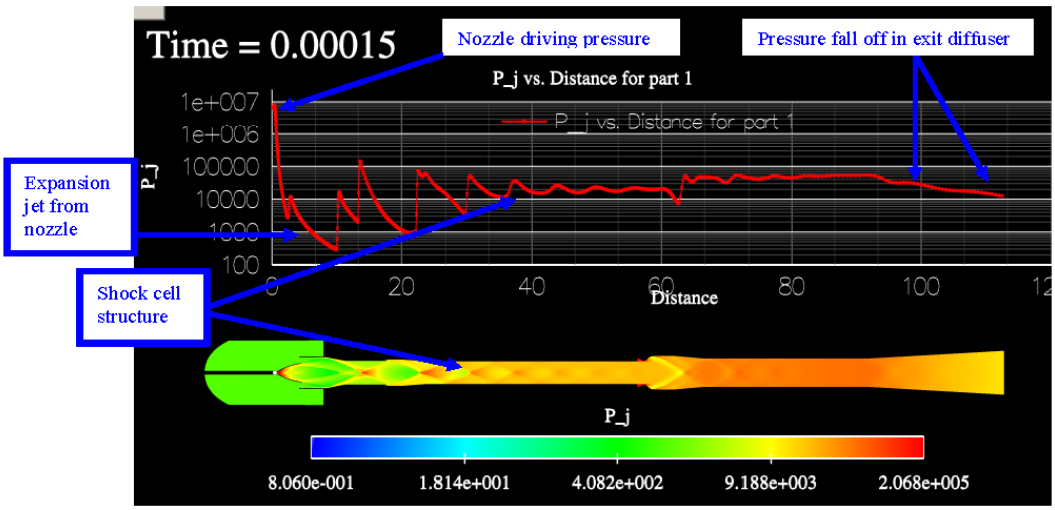

Figure 2. Centerline pressure distribution matched up against pressure distribution and physical location in the facility.

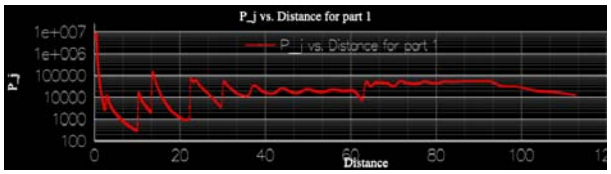

Time = 0.00015

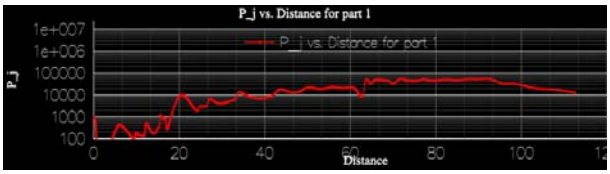

Time = 0.01289

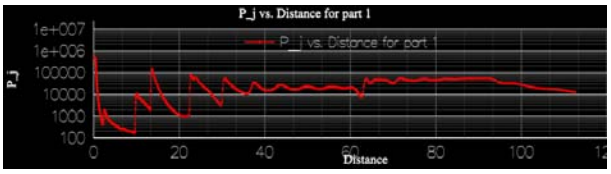

Time = 0.00261

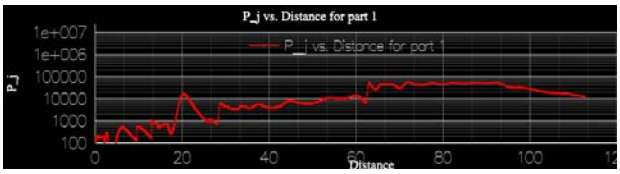

Time = 0.01901

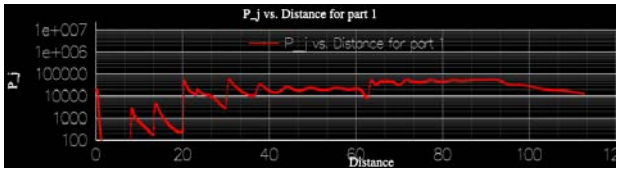

Time = 0.00684

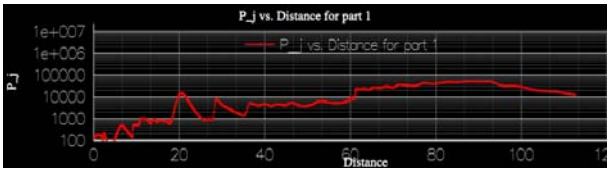

Time = 0.02597

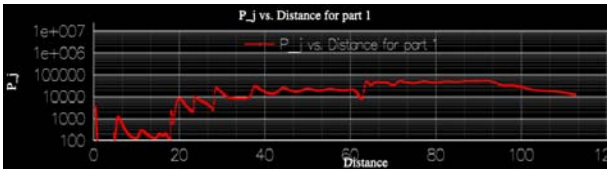

Time = 0.00960

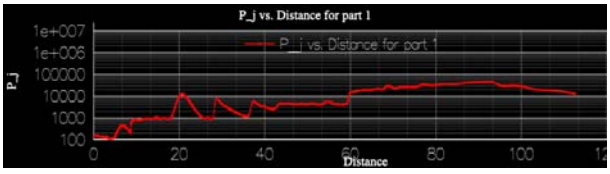

Time = 0.03223

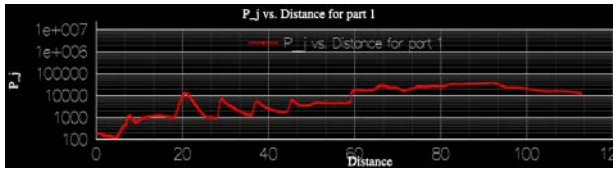

Time = 0.03958

Figure 3. Sequence of centerline pressure plots showing pressure variation along the axis during engine shutdown.

Computational Analyses in Support of Sub-scale Diffuser Testing for the A-3 Facility – Part 2: Unsteady Analyses and Risk Assessment

Vineet Ahuja[1], Ashvin Hosangadi[2], Andrea Zambon[3] and James Erwin[4]
Combustion Research and Flow Technology, Pipersville, PA 18947

and

Daniel Allgood[5]
NASA Stennis Space Center, MS 39529, USA

This paper is the second of a three part series which investigates the computational modeling requirements for a new altitude rocket test facility. The focus of this paper is to demonstrate the role that simulations can play in supporting the design and development of the test facility by assessing risks, providing analysis of dynamic pressure and thermal loads, identifying failure modes and predicting the anomalous behavior of critical sub-systems. Two separate studies were performed of the facility in different modes of operation. In the first study, transient simulations were carried out which represented a nominal engine shutdown process. In the second study, the risk of afterburning due to mixing between the fuel rich engine plume and oxygen emissions from the chemical steam ejectors was evaluated using a chemically reacting simulation. The possibility of facility un-start due to afterburning in the diffuser flow path was identified.

I. Introduction

The President's vision for space exploration called for manned missions to the Moon and Mars leading to the design and development of two new transport vehicles namely the ARES V and the ARES I. The primary propulsion element of ARES I and the Earth Departure Stage (EDS) of ARES V will consist of the J-2X engine that has evolved from the J-2 engine that was used in the Saturn program. Unlike the SSME engines that are ignited at lift-off, flight plans call for the J-2X upper stage engine to be ignited at 133.7 seconds after lift-off at an altitude above 177,000 feet. As a consequence, certification and testing of the J-2X engines have to be performed under environmental conditions that mimic conditions the engine is exposed to during upper stage ignition and high altitude flight operations. There are significant challenges associated with extensive testing of engines of the 300k lbf thrust class such as the J-2X engine at high altitude conditions. The A-complex facilities at NASA Stennis Space Center(SSC), where SSME altitude tests are performed, are presently limited in scope to altitude testing, and thus a new facility (A-3) is under construction to meet the new requirements for altitude testing for the J-2X engine. The proposed design includes steam ejectors, a supersonic diffuser, an exit diffuser and a turning duct and is very different from existing facilities at SSC. Design issues under consideration with the A-3 facility include: (a) the performance of the supersonic diffuser duct and the issues related to "un-start modes" especially under flow transients during startup and shutdown, (b) issues related to maintaining low pressure in the test chamber with the steam ejector trains, (c) plume aspiration flow dynamics in the test facility that includes flow through the turning duct and heat transfer issues related to turning a primarily supersonic plume, (d) entrainment of flow from test chamber prior to startup and interaction of initial blast wave with the steam ejectors, (e) purge and pressure control in the upstream chamber as well as steam ejector performance especially during shutdown including evaluation of

[1] Senior Research Scientist, 6210 Keller's Church Rd., and AIAA Senior Member. Email:*vineet@craft-tech.com*
[2] Principal Scientist, 6210 Keller's Church Rd., and AIAA Senior Member.
[3] Research Scientist, 6210 Keller's Church Rd., and AIAA Member.
[4] Research Scientist, 6210 Keller's Church Rd., and AIAA Member.
[5] Aerospace Technologist, Stennis Space Center, MS 39529-6000, and AIAA Senior Member.

the possibility of blow-back, and (f) performance of chemical steam generators and the interaction of their predominantly steam exhaust flow with the test-article plume.

Simulation technology can play an important role in the rocket engine testing environment by providing design support, assessing risks, providing analysis of dynamic pressure and thermal loads, identifying failure modes and predicting anomalous behavior of critical systems. In a companion paper[1], we have demonstrated, with the use of CFD, the capability of performing steady analyses of the supersonic diffuser flow path for the purposes of evaluating the nominal performance of a sub-scale A-3 facility. However, there are significant transient issues related to the performance and operation of the facility especially at startup and shutdown. For example, the entrainment of the air in the test chamber by the steam ejectors prior to engine startup is purely a turbulent mixing process and is driven by the ratio of the total pressure at the ejector exit to that of the entrained air-stream. Analysis based on the ejector driving pressure, ejector nozzle configuration, operating temperature and facility design needs to be carried out to evaluate the efficacy of the entrainment process and time required to evacuate the facility to the operating altitude pressure levels. On the other hand, the shutdown process in the facility, either as a controlled event or a result of an aborted test can result in significant blow-back and pressure loading on the engine resulting in serious damage. The placement of the steam ejectors and their operating envelope is usually designed for such cases in pressurizing the facility and alleviating any large scale pressure fluctuations that might result from an abort related shutdown.

Lastly, the performance of the steam ejectors/chemical steam generators is critical not only during startup/shutdown of the rocket engine but also during the duration of the test. The interaction of the supersonic streams, i.e., rocket engine plume with flow from the steam ejector is replete with important flow physical phenomena such as shock boundary layer interaction, annular supersonic mixing, shock-shock interaction and interaction between the variable area ducting with the supersonic streams. Total pressure ratio between the streams, relative Mach number, and the amount of area contraction and expansion play a significant role in determining the resultant flow in the facility. Issues with these chemical steam generator units relate to the efficiency of the combustion process, resultant emissions and the interaction of any resultant un-burned oxygen with the fuel rich plume in a confined facility.

In this paper, we will carry out two separate studies with the help of numerical simulations to address transient issues with the operation of the facility especially at facility shutdown, and assess risks related to afterburning due to the interaction of a fuel rich plume with oxygen that is a by-product of the steam ejectors. The first numerical study looked at the engine shutdown event with special emphasis on engine loading. This study was carried out on a simplified model of the full scale A-3 facility (Figure 1a) by removing the turning duct. The second study assessed the risk of afterburning in the facility with reacting CFD simulations and for this simulation the sub-scale A-3 test facility (Figure 1b) was utilized since a facility *un-start* event was observed during testing in the sub-scale facility. In the next section, we provide a brief review of the numerical formulation and the computational framework. This is followed by a discussion of the two above-mentioned studies. The paper concludes with a summary of the work that was performed and the lessons learned thereof.

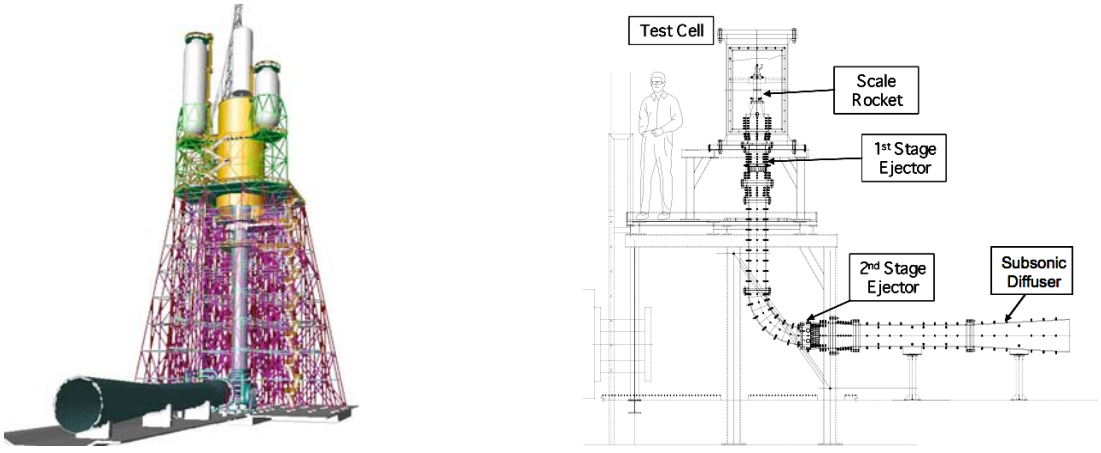

(a) (b)

Figure 1. (a) Schematic of the A-3 Test Stand and (b) the Sub-scale A-3 Test Facility.

II. Numerical Framework

A. Equations and Basic Numerics

The CRUNCH CFD® code[2-4] is a hybrid-element (i.e. tetrahedral, prismatic, pyramid, and hexahedral cells) unstructured flow solver for viscous, real gas systems. It allows for generalized thermo-chemistry specification, permits dynamic grid motion, and has a coupled two-equation turbulence model (see Table I for a list of features). CRUNCH is formulated for an edge-based data framework (following Barth[5,6]) where the solution is saved at the cell-vertex and a dual control-volume is defined by cutting across all edges coming to a node. Such an edge-based formulation is attractive when dealing with multi- elements since the dual surface associated with an edge can include contributions from different element types resulting in a "grid transparent" framework for inviscid flows. For efficient computation of large 3D problems, a parallel framework for distributed memory systems has been implemented along with a sparse matrix solvers (GMRES and Gauss-Seidel procedures) thereby providing a robust computational tool for complex three-dimensional applications.

Table I. CRUNCH CFD® Navier-Stokes Code Features.

NUMERICS	• Finite-Volume Roe/TVD Flux Construction, Vertex Storage
INTEGRATION	• Explicit Four-Step Runge-Kutta, Implicit GMRES, Gauss-Seidel
GRID ELEMENTS	• Tetrahedral, Hexahedral, Prismatic, Pyramid
PARALLEL PROCESSING CAPABILITIES	• Domain Decomposition MPI, Independent Grids with Noncontiguous Interfacing, Automated Load Balancing
DYNAMIC GRID CAPABILITIES	• Node Movement Solver (Implicit Elasticity Approach), Automated Embedding, Sliding Interfaces
GRID ADAPTION	• Variable Element Grid Refinement using Delaunay and cell subdivision Procedures, Automated Load Balancing of Adapted Grid
THERMOCHEMISTRY	• Multi-component Real Gas Mixtures, Finite-Rate Kinetics
TURBULENCE RANS/LES	• $k\tilde{\varepsilon}$ /EASM Formulations with Compressibility/Vortical Upgrades • LES Subgrid Scale Models – Algebraic and One-equation • Algebraic (Smagorinsky) and Single Equation (k) SGS Models
MULTIPHASE FLOW	• Non-equilibrium Particle/Droplet Solvers (Eulerian and Lagrangian Formulations)
NUMERICS	• Finite-Volume Roe/TVD Flux Construction, Vertex Storage
INTEGRATION	• Explicit Four-Step Runge-Kutta, Implicit GMRES, Gauss-Seidel

The governing equations are written in finite-volume form for each vertex dual as follows:

$$\frac{\partial}{\partial t}\int_{\Omega} Q\,dV + \int_{\partial\Omega} F(Q,n)\,ds = \int_{\partial\Omega} G(Q,n)\,ds + \int_{\Omega} D\,dV \qquad \textbf{(1)}$$

Following the standard notation, Q is the vector of dependent variables, F (Q, n) is the inviscid flux vector, G(Q,n) is the viscous flux vector, and D is the chemical/turbulent source term. The vectors Q,F,G,D are defined as

$$Q = \left[\rho, \rho u, \rho v, \rho w, E, \rho_1, \ldots, \rho_s, \ldots, \rho_{NS-1}, \rho k, \rho\varepsilon\right]^T \qquad (2)$$

$$F(Q,n)=\begin{bmatrix}\rho(U-U_r)\\ \rho(U-U_r)u+n_xP\\ \rho(U-U_r)v+n_yP\\ \rho(U-U_r)w+n_zP\\ (E+P)U-EU_r\\ \rho_i(U-U_r)\\ \vdots\\ \rho_{NS-1}(U-U_r)\\ \rho k(U-U_r)\\ \rho\varepsilon(U-U_r)\end{bmatrix} \qquad \vec{G}=\begin{bmatrix}0\\ \tau_{xx}\\ \tau_{yx}\\ \tau_{zx}\\ \tau e_x\\ q_x^s\\ q_x^{s_1}\\ \vdots\\ q_x^{s_{NS-1}}\\ q_x^k\\ q_x^\varepsilon\end{bmatrix}\hat{i}+\begin{bmatrix}0\\ \tau_{xy}\\ \tau_{yy}\\ \tau_{zy}\\ \tau e_y\\ q_y^s\\ q_y^{s_1}\\ \vdots\\ q_y^{s_{NS-1}}\\ q_y^k\\ q_y^\varepsilon\end{bmatrix}\hat{j}+\begin{bmatrix}0\\ \tau_{xz}\\ \tau_{yz}\\ \tau_{zz}\\ \tau e_z\\ q_z^s\\ q_z^{s_1}\\ \vdots\\ q_z^{s_{NS-1}}\\ q_z^k\\ q_z^\varepsilon\end{bmatrix}\hat{k} \tag{3}$$

where

$$\begin{aligned}\tau e_x &= \tau_{xx}u+\tau_{xy}v+\tau_{xz}w-q_x^h+\sum_{i=1}^{NS-1}(h_i-h_{NS})q_x^{S_i}\\ \tau e_y &= \tau_{yx}u+\tau_{yy}v+\tau_{yz}w-q_y^h+\sum_{i=1}^{NS-1}(h_i-h_{NS})q_y^{S_i}\\ \tau e_z &= \tau_{zx}u+\tau_{zy}v+\tau_{zz}w-q_z^h+\sum_{i=1}^{NS-1}(h_i-h_{NS})q_z^{S_i}\end{aligned} \tag{4}$$

The first five equations represent global continuity, momentum, and energy equation; the next (NS-1) equations represent species continuity; and, the last two equations represent scalar transport of turbulent kinetic energy and dissipation rate.

The inviscid flux procedure involves looping over the edge list and computing the flux at the dual face area bisecting the edge. A Riemann problem is solved for using higher order reconstructed values at the dual face (see Ref. [2] for details). Presently, a second-order linear reconstruction procedure (following Barth[5]) is employed to obtain a higher order scheme. The higher-order variables need to be limited to yield a TVD scheme. We note that the inviscid flux procedure as outlined here is grid transparent; given a dual area associated with each edge the details of the different element types contributing to this edge are not relevant.

The viscous fluxes are computed by estimating the gradients (or stresses) at the cell faces and then performing a Green-Gauss integration of the stresses around each dual volume (see Ref. [3] for details). For hexahedral cells where the edge vectors are not skewed relative to the cell faces, an edge-based viscous flux procedure can be derived. However, for tetrahedral cells where edge skewness is substantial, the edge based procedure fails, particularly for the k-ε equations, and is reflected in incorrect turbulent viscosity levels. For tetrahedral cells, a cell based procedure has been implemented which remedies this problem.

B. Chemical Kinetics Extensions

The scalar equation extensions described in the previous section permit the analysis of generalized, multi-component gaseous flow-fields including real gas behavior. Source terms added to these equations permit the analysis of non-equilibrium phenomena associated with finite rate chemical kinetics. The chemical kinetics are modeled in a completely general fashion[2] where an arbitrary set of reactions may be specified by the user. The source term vector, D, is written as:

$$D=\left(0,0,0,0,0,\dot{\omega}_1,\dot{\omega}_2,\ldots,\dot{\omega}_{ns-1}\right)^T \tag{5}$$

where $\dot{\omega}_s$ is the chemical source term for the production of species, s, resulting from any number of chemical reactions involving that species. We presently restrict our attention to conventional "laminar chemistry" given by the law of mass action

$$\dot{\omega}_s = M_s \Sigma\left(\nu'' - \nu'\right)\left[K_f \Pi\alpha^{\nu'} - K_b \Pi\alpha^{\nu''}\right] \tag{6}$$

where α is the molar concentration of species s given by

$$\alpha_s = \rho_s / M_s \tag{7}$$

The forward and backward reaction rates (K_f and K_b) are a function of temperature and are expressed in modified Arrhenius form as:

$$K(T) = \exp\left(\ell n\, C_1 + C_2 / T + C_3 \ell n\, T\right) \tag{8}$$

where C_1, C_2, and C_3, are reaction rate coefficients for each reaction.

The species scalars currently are solved strongly coupled with the fluid equations. For implicit sparse solvers, the large block size of the matrices makes this a very memory intensive procedure. A new solution procedure where the species convection terms are weakly coupled is currently being investigated.

C. Turbulence Modeling

The 'standard' high Reynolds number form of the *k-ε* equations forms the basis for turbulence modeling in CRUNCH CFD. Transport equations for the turbulent kinetic energy and its dissipation rate are solved along with the basic momentum and energy equations. These equations, with supplemental low Re and terms, are as follows,

$$\frac{\partial \rho k}{\partial t} + \frac{\partial}{\partial x_i}\left(\rho u_i k - \left(\mu + \frac{\mu_T}{\sigma_k}\right)\frac{\partial k}{\partial x_i}\right) = P_k - \rho\varepsilon + S_k$$

$$\frac{\partial \rho \varepsilon}{\partial t} + \frac{\partial}{\partial x_i}\left(\rho u_i \varepsilon - \left(\mu + \frac{\mu_T}{\sigma_\varepsilon}\right)\frac{\partial \varepsilon}{\partial x_i}\right) = C_1 f_1 P_k - C_2 f_2 \rho\varepsilon + S_\varepsilon$$

$$\mu_T = C_\mu f_\mu \rho \frac{k^2}{\varepsilon} \tag{9}$$

where, σ_k, σ_ε, C_1 and C_2 are the modeling constants, and f_1,f_2, f_μ are low Re (near-wall) empirical modeling functions which equal unity in the high Reynolds number form.

Corrections to k-ε may be required to account for the effects of compressibility. A compressible wall function serves as a baseline method for near-wall analysis but does not perform adequately for highly separated regions. Extended variants of k-ε that account for non-linear effects may be required to handle the complex vortical physics seen in scramjets. Three primary upgrades have been implemented in CRUNCH namely: (1) n^+ based near wall low Reynolds number models to enable integration to the walls; (2) compressibility corrections of Sarkar to account for effects of compressible-dissipation and pressure-dilation; and (3) an Explicit Algebraic Stress Model (EASM) to include non-linear effects. These extensions are described in reference [4]. The EASM model, in particular, is shown to significantly improve predictions in complex vortical flow regions, by allowing the model parameter Cμ to vary as a function of the local flow conditions, as opposed to being a constant as in the traditional k-ε models. Developmental work includes accounting for variable Pr_t/Sc_t effects (see Ref. [7]) and using PDF turbulent combustion models (see Ref. [8]).

III. Results and Discussion

A. Simulation of Engine Shutdown in Approximated A-3 Facility

Unsteady simulations have been carried out to study the engine-shutdown process in the facility and understand the physics behind the interactions between the steam ejectors, the test cell and the supersonic diffuser. As a first approximation, the turning duct in the facility was removed from the model. The main components of the facility such as the test cell, engine/nozzle profile, the supersonic diffuser, the first and second stage ejectors and the exit diffuser have been retained and in general correspond to the actual facility with the sole exception of the turning duct (see Figure 2). This simplification of the facility was primarily done to facilitate an axisymmetric approximation thereby reducing the computational time required and still capture most of the important flow dynamics that affect the engine-shutdown process.

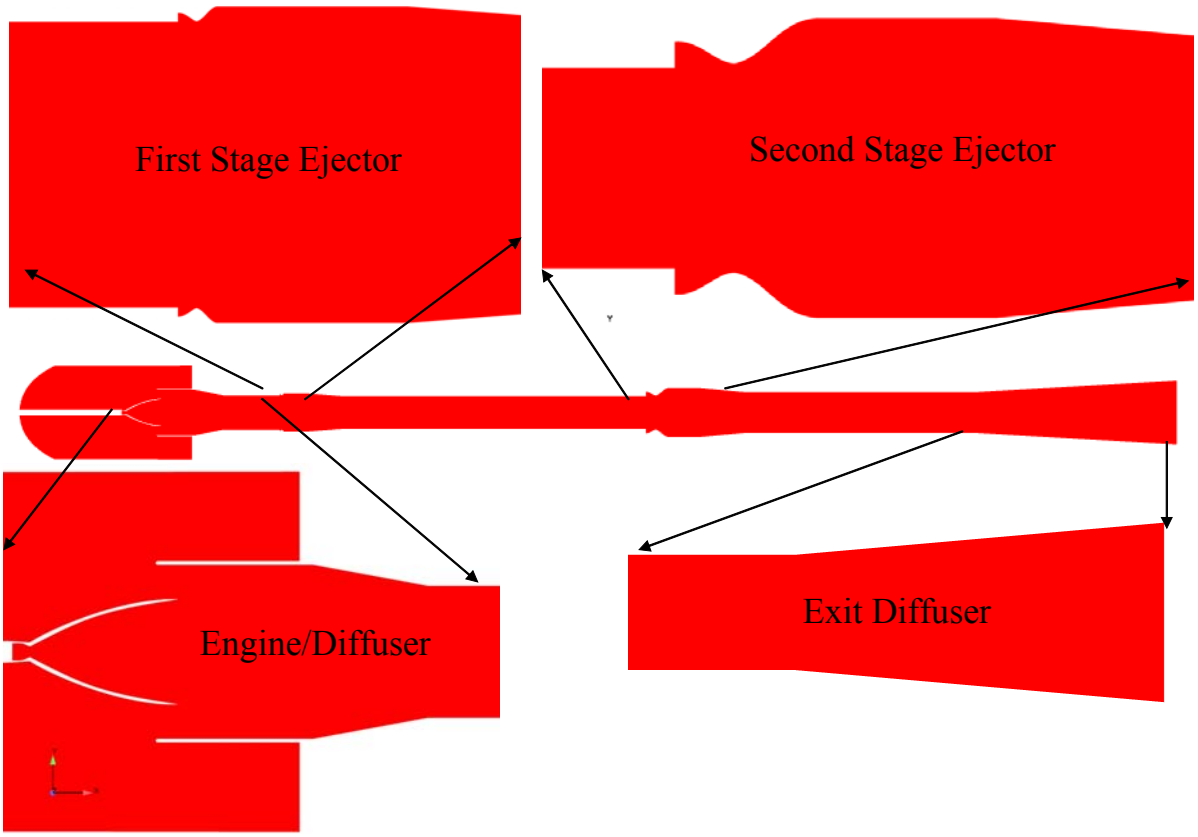

Figure 2. Simplified Model of the A-3 Facility Utilized for Engine-Shutdown Simulation

The following section of the paper provides a detailed discussion of the flow dynamics observed in the engine-shutdown analysis. The engine shutdown process was initiated by impulsively turning off the mass flow from the engine nozzle inflow boundary. The pressure at the boundary was computed from solving the momentum conservation equations and did not instantaneously drop. Rather it dropped from the nominal combustion chamber pressure of 1337 psia to the test cell pressure of 0.16 psia in approximately 12.89 milli-seconds. The evolution of the flow is shown in Figure 3 where a series of snapshots of Mach number distributions in the facility are shown. As the engine lost its power, and consequently the chamber pressure dropped, the strong under-expanded jet from the engine nozzle weakened and turned parallel to the jet axis after 6.84 msec. This triggered an expansion wave that traveled downstream through the supersonic diffuser section. As the expansion wave traveled downstream, the strong pressure gradient between the test cell and the section of the supersonic diffuser close to the nozzle exit drove the flow from the test cell into the supersonic diffuser towards the central axis. The flow entrainment from the test cell re-pressurized the supersonic diffuser section just downstream of the nozzle exit and a small amount of backflow entered the nozzle after approximately 9.6 msec.

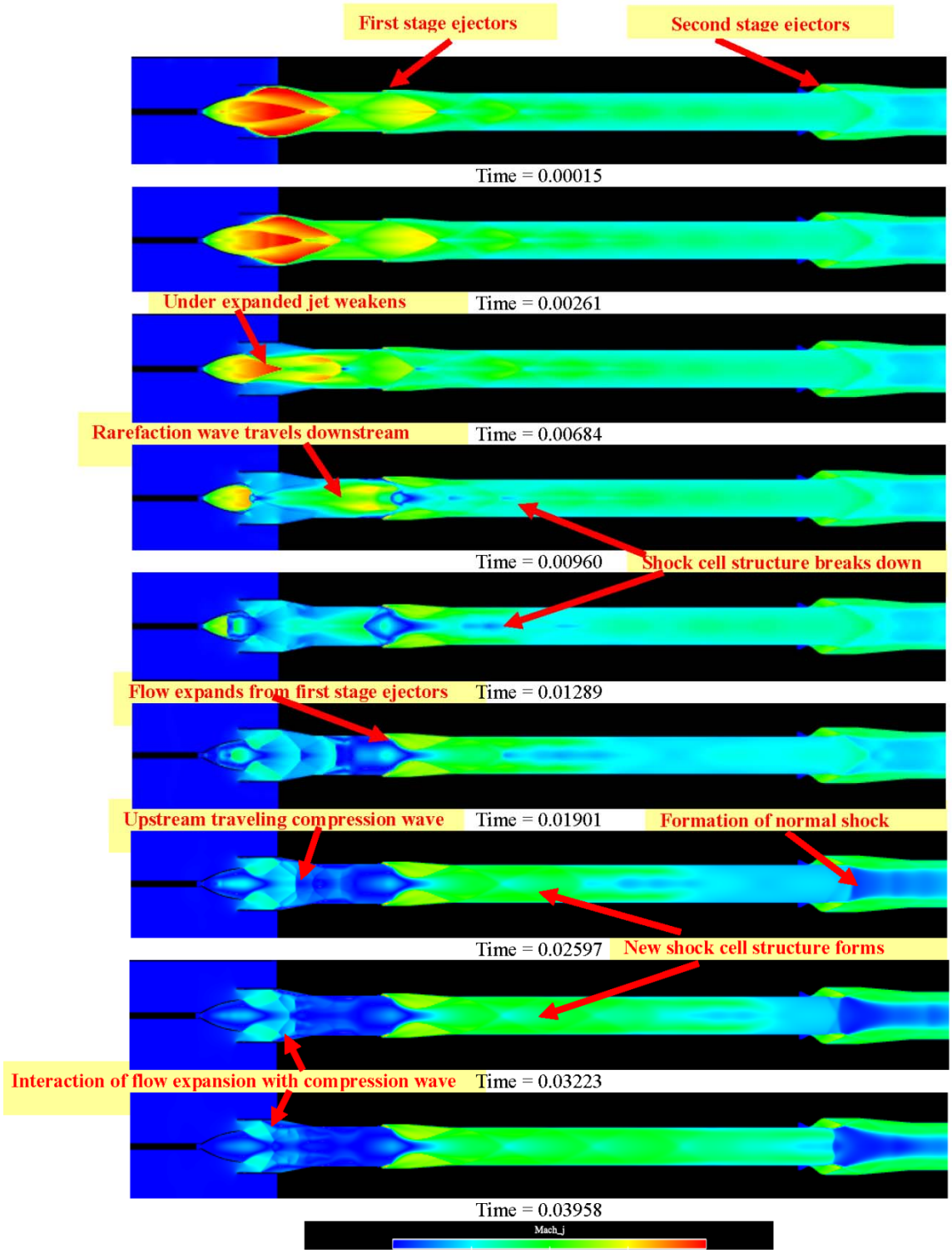

Figure 3. Sequence of Mach Number Distributions Showing Evolution of Flow in the Facility During Engine Shutdown

As the rarefaction wave traveled downstream of the first stage steam ejectors, it changed the shock cell structures in the region of the diffuser duct between the first stage and second stage steam ejectors. Effectively, the deviation angle of the shock cells steepened which gave the impression that the shock cell structures were moving upstream as it was weakening. Flow from the first stage ejectors responded by expanding towards the diffuser centerline and

eventually formed a new shock train in the diffuser duct between the first and second stage ejectors. This can be seen in Figure 3 at approximately 19msec into engine shutdown.

The complete expansion of the first stage ejectors to the diffuser duct centerline produced a backward propagating compression wave which traveled upstream from the first stage ejector plane towards the engine nozzle. This compression wave first interacted with the expansion wave formed near the corner of the supersonic diffuser where the area contraction straightens out. Moving upstream it then interacted with the oblique shock near the diffuser wall where the diffuser area contracts. Finally, the upstream propagating compression wave had a complex interaction with the flow expanding from the test cell near the exit plane of the nozzle and remnants of flow from the nozzle at approximately 40msec into engine shutdown.

Meanwhile, as the flow in the duct between the first and second stage ejectors settled into a new shock train pattern, the pressurization across the plane of the second stage ejector changed near the centerline in the core flow. As a consequence, the oblique shock near the centerline close to the plane of the second stage ejector steepened till it turned into a normal shock. Thus the shock train in the duct between the first stage and second stage ejectors transitioned into a normal shock by the second stage ejectors. It is important to note here that in the evaluation of these transient flow processes during engine-shutdown, it was evident that the flow in the facility past the first stage ejector plane remained supersonic throughout the shutdown process. This signified successful isolation of the engine from the external surroundings. If the flow in the diffuser duct upstream of the second stage ejector had turned subsonic, then the ambient sea-level pressure of the surroundings would have been able to prematurely communicate back to the engine and test cell resulting in a destructive high pressure loading on the engine nozzle.

Figures 4 and 5 show line plots of pressure distribution along the centerline of the diffuser duct matched against the location and pressure distribution in the facility. The line plots are plotted in a log scale to accommodate the large variation in pressure between the nozzle at full power to the low pressures seen near the nozzle after shutdown. The pressure line plots clearly show the pressure dropping in the engine and the downstream traveling rarefaction wave indicated by the weakening (smaller amplitudes) of the oblique shocks in the diffuser section just aft of the nozzle. Furthermore, we also see the weakening of the shock cell structure in the diffuser duct between the first and second stage ejectors, and the reformation of a new shock cell structure in the duct as the flow from the first stage ejector expanded radially outward to the diffuser duct centerline. The formation and eventual migration of the upstream traveling compression wave from the first stage ejectors can also be seen in these figures. Both the first and second stage ejectors were seen to pressurize the diffuser duct and maintain fairly constant pressure levels. As a result, the pressure distribution in the exit diffuser did not change much during the shutdown process. This was indicative of the fact that both the ejector stages were performing satisfactorily and prevented any blow-back or large scale pressure fluctuations from entering the engine. Specifically, the pressure loading in and around the nozzle after engine shutdown was fairly small, where average pressures ranged between 100-200 Pa (0.015-0.029 psia) as seen in the centerline pressure plots.

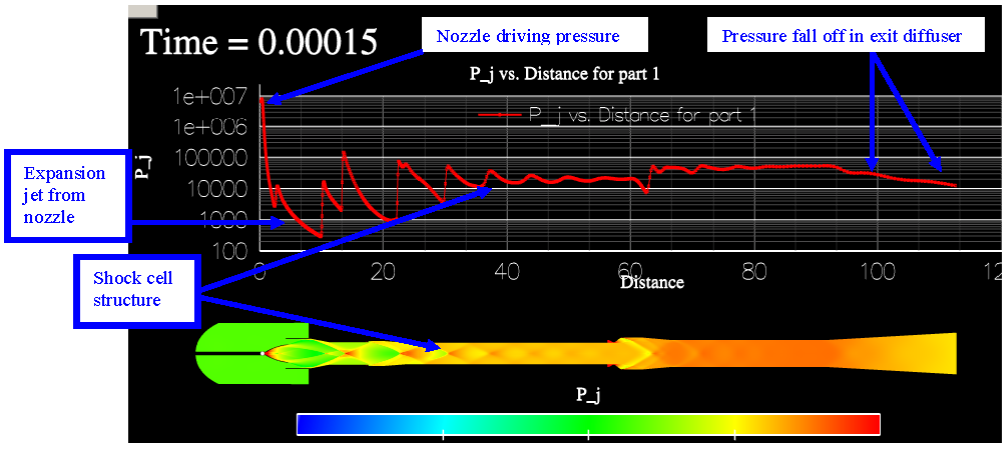

Figure 4. Diffuser Centerline Pressure Traces and Corresponding Facility Pressure Distributions at 0.15msec After Engine-Shutdown

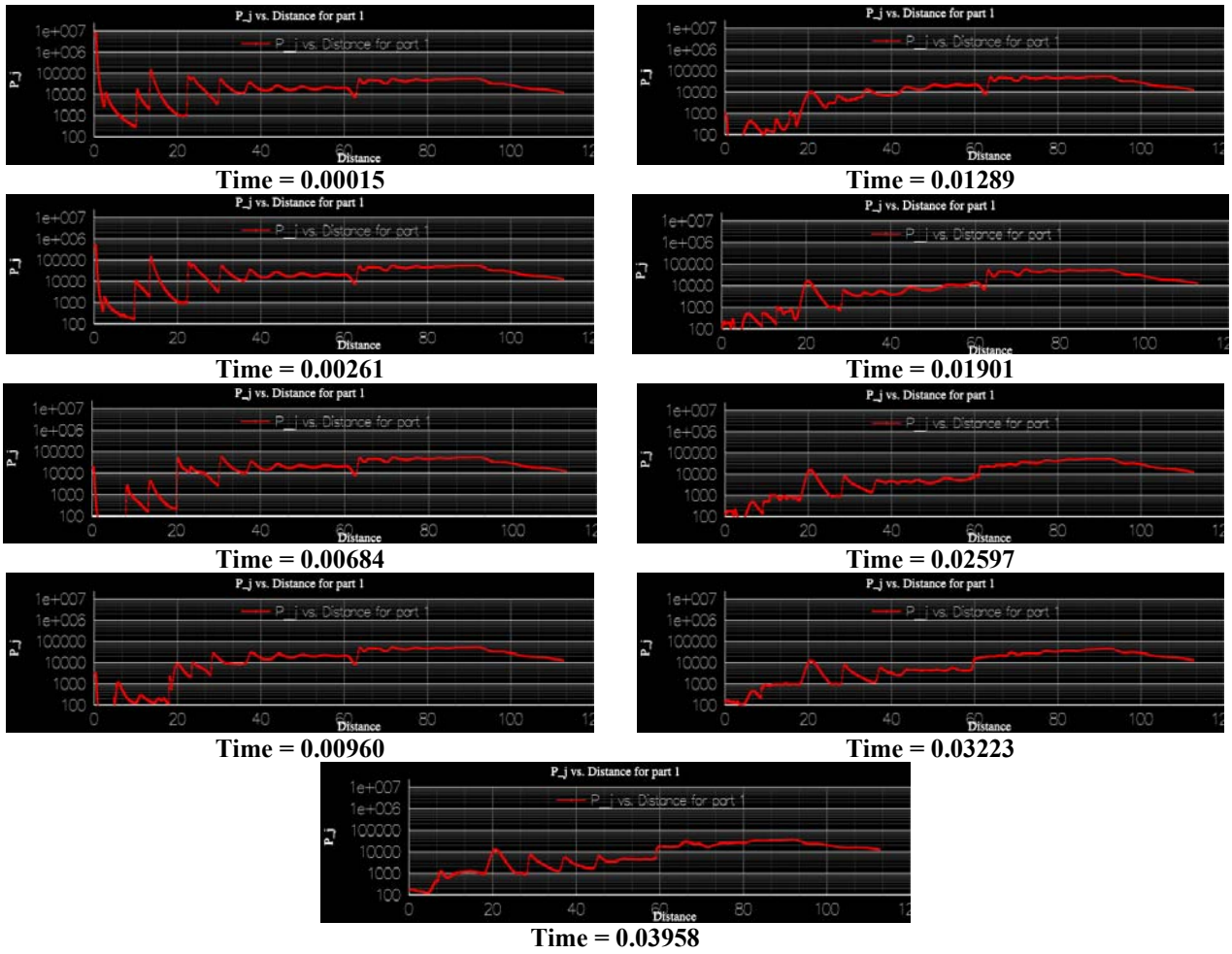

Figure 5. Sequence of Diffuser Centerline Pressure Traces Showing Pressure Variations Along the Diffuser Axis During Engine-Shutdown

B. Afterburning Simulation in Sub-scale A-3 Diffuser

Reacting flow simulations were carried out for the A-3 subscale facility to study the possibility of afterburning in the facility diffuser duct given a fuel-rich engine plume and excess un-burned oxygen being emitted as a by-product from the chemical steam ejectors. Finite-rate chemical kinetics for the H_2/O_2 system is modeled with a JANNAF mechanism comprising of 7 species in 8 elementary reactions. Based on equilibrium calculations using the NASA Chemical Equilibrium Analysis (CEA) code, there are 6 primary species (H_2O, O_2, H_2, H, O, and OH) present in the subscale J-2X engine combustion chamber with some additional trace species corresponding to the nominal 100% rocket power level operating conditions. In the CFD analysis, the fluid was modeled as a composition of these species with the remaining trace species being approximated as an inert species (N_2). The CEA code predicted a species composition in the sub-scale engine combustion chamber of 90.87% water vapor, 4.773% hydrogen, 3.6% OH radicals, and trace amounts of oxygen, atomic oxygen and nitrogen. The above-mentioned species composition, combined with a total pressure of 1337psia and stagnation temperature of 5714 deg. F, were the imposed inflow boundary conditions in the engine for the CFD reacting flow simulation. The species composition at the exit of the converging-diverging steam ejector nozzles for the first and second stages were assumed to be composed of primarily water with a non-negligible percentage of excess oxygen. It is important to note here that these simulations do not represent the full-scale facility as the chemical steam generators for the full-scale operate using a hydro-carbon fuel. Rather, these species concentrations are representative of one of the many tests performed during the sub-scale risk mitigation program at NASA Stennis.

The mechanism for afterburning in the sub-scale diffuser duct can be explained with the help of Figures 6 and 7. Figure 6 shows that in a non-reacting multi-species simulation, the distribution of hydrogen species in the facility diffuser duct was primarily concentrated around the central axis of the diffuser until it approached the turning duct. Likewise, the oxygen species distribution in Figure 7 shows that un-burned oxygen exhausted from the first stage chemical steam ejector train had its highest concentration close to the walls of the facility. There was as such very little mixing between the two supersonic streams (plume from engine and first stage ejector exhaust) in the vertical section of the facility. As the flow approached the turning duct, the supersonic core flow in the diffuser (primarily hydrogen gas) resisted turning and impinged on the outer wall of the turning duct. The flow separated from the inside turn of the diffuser thereby enhancing the mixing between the hydrogen and oxygen. Localized high temperature regions along the outer wall of the turning duct, as a consequence of shock formation at the mitered joints, acted as ignition sources for the combustible mixture of un-burned oxygen and hydrogen. A second combustion zone was also formed by the Mach disk just downstream of the second stage ejectors. Figure 8 is an illustration of the flame fronts that are formed in the turning duct and near the second stage ejectors. These flame fronts are illustrated in the figure by iso-surfaces of OH concentration.

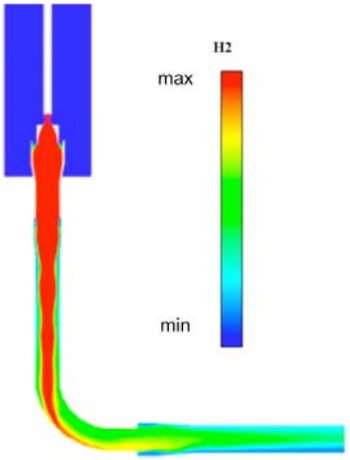

Figure 6. Hydrogen Species Mass Fraction Distribution in the Sub-scale Diffuser

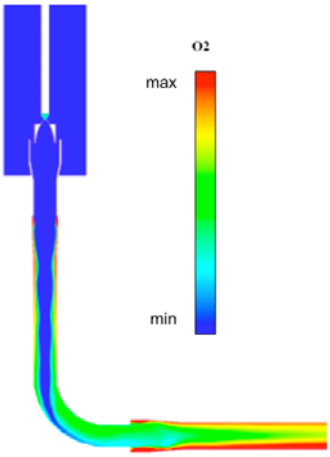

Figure 7. Oxygen Species Mass Fraction Distribution in the Sub-scale Diffuser

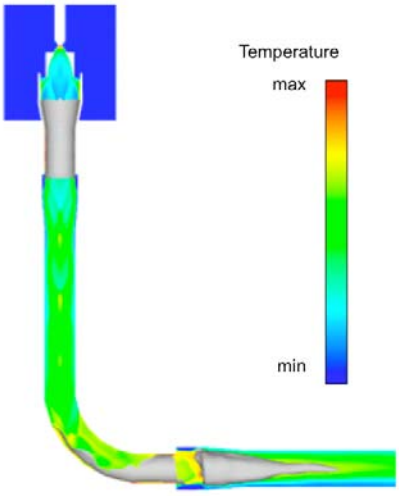

Figure 8. Iso-surface of OH Species Concentration Showing the Formation of Combustion (Heat-Release) Zones in the Sub-scale Diffuser

The OH species distribution along the central plane of symmetry in the facility is shown in Figure 9. There are a few important points the authors would like to note first regarding the OH concentrations observed upstream of the turning duct. First, given the high temperature field in the core of the engine plume, certain amounts of dissociation of hydrogen and water vapor occurred leading to the formation of OH. Secondly, there was a slight increase in OH concentration near the shock structures in the supersonic diffuser upstream of the first stage ejectors due to the shock induced increase in temperature. Lastly, the high temperature boundary layers also showed formation of OH due to dissociation of water. However, none of these OH formation zones represented significant heat release or afterburning.

Although the increase in OH radicals upstream of the turning duct had little effect on the flow-field in this region, these radicals did serve to enhance the combustion in the well-mixed oxygen-hydrogen zone within the turning duct. The Mach number distribution along the central plane of symmetry is shown in Figure 10. The Mach number distribution was plotted on two different scales to highlight the fact that the flow in the turning duct and downstream of the second stage ejectors had turned predominantly subsonic leading to *un-start* of the facility.

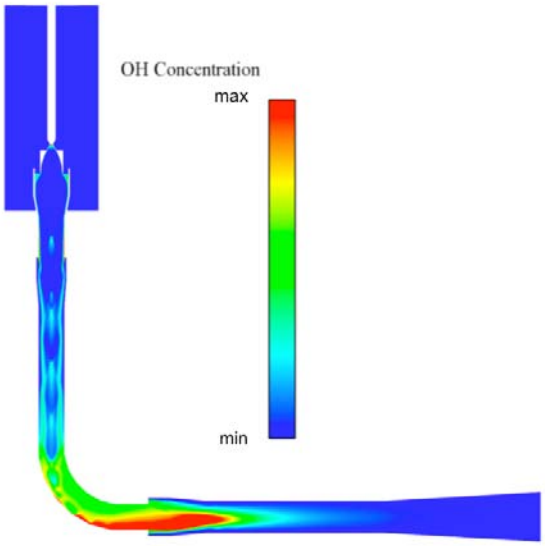

Figure 9. OH Mass Fraction Distribution in the Sub-scale Diffuser as Predicted by the Afterburning Simulation

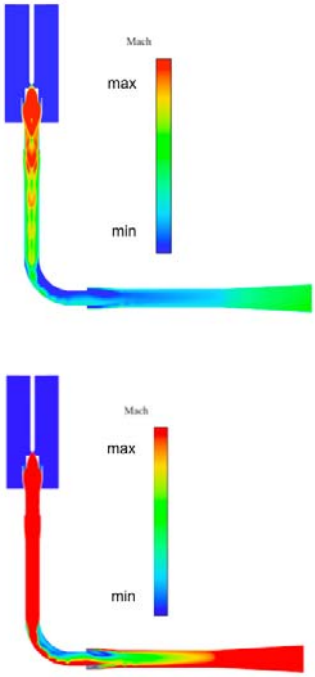

Figure 10. Mach Number Distribution in the Sub-scale Diffuser as Predicted by the Afterburning Simulation

A comparison of the temperature distribution (Figure 11) between the afterburning simulation and the corresponding frozen simulation (without chemical reactions) shows the impact of heat release due to combustion. The temperature in the turning duct has risen considerably (on average by 500K). Furthermore, a comparison of the pressure distribution (Figure 12) also shows an increase in pressure in the turning duct (4 psia on average) as well as the horizontal duct (6 psia on average). These simulations show that with the present assumed excess concentration of un-burned oxygen emitted from the chemical steam ejectors, there is a potential for *un-start* in the facility due to heat release from combustion in the turning duct. Additional simulations, not reported in the current work, have demonstrated that ejector flows with a tenth of the present oxygen concentration produced a much smaller combustion zone due to the insufficient oxygen to combust with the excess hydrogen from the engine. Furthermore, the low-levels of heat release generated for this condition of low-oxygen concentration steam flow, did not lead to a facility *un-start* condition.

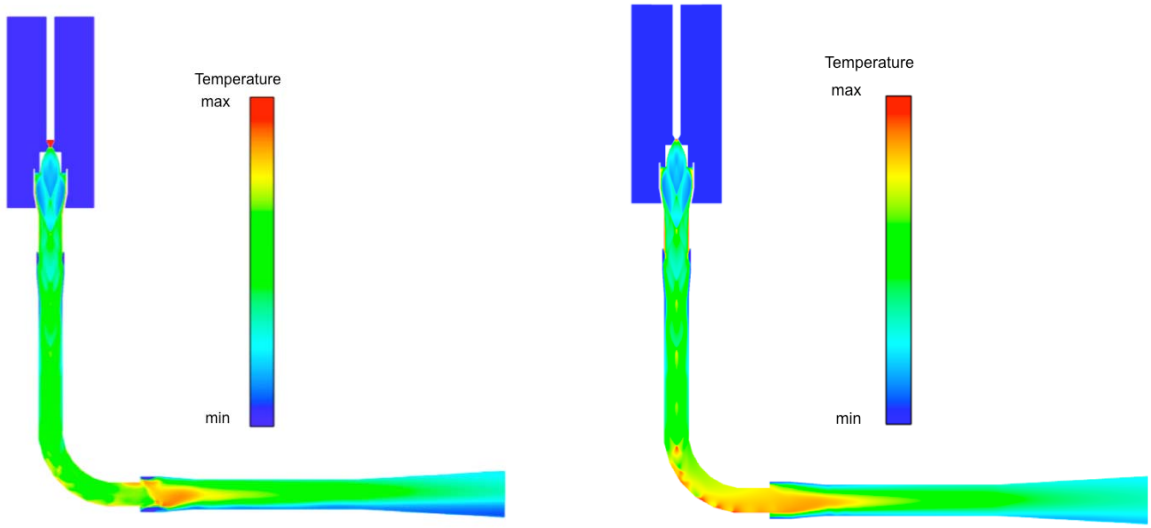

Temperature (without afterburning) Temperature (with afterburning)

Figure 11. Comparison of Temperature Distributions for the Sub-scale Diffuser With and Without Afterburning

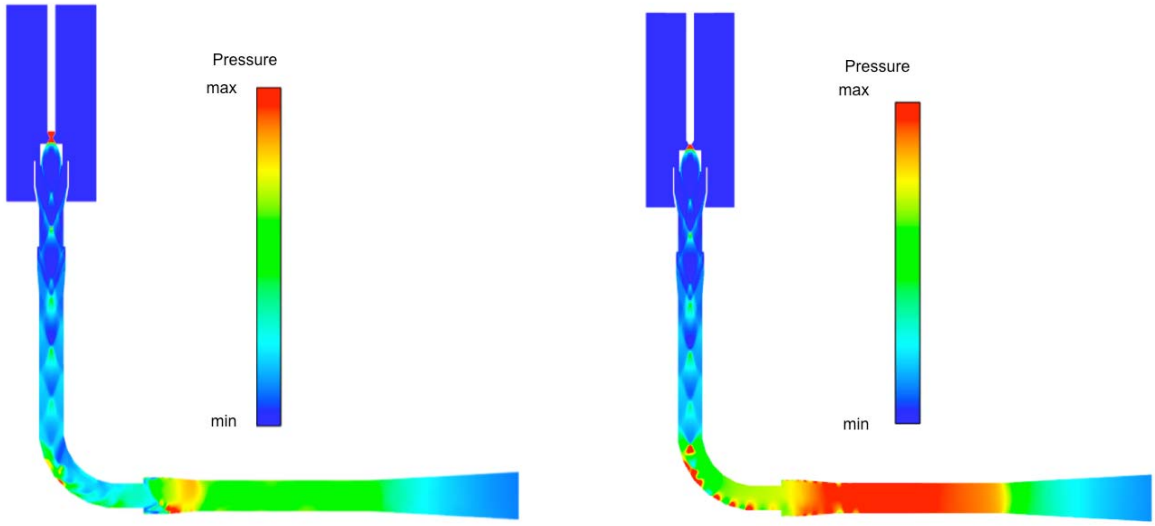

Pressure (without afterburning) Pressure (with afterburning)

Figure 12. Comparison of Pressure Distributions for the Sub-scale Diffuser With and Without Afterburning

IV. Summary

This paper is the second paper in a three part series that looked into numerical analyses as a design support tool for a steam driven high altitude facility being constructed at NASA SSC. In the first paper, the groundwork was laid in terms of modeling approximations for the steam ejector nozzles and the steady-state nominal operating conditions of the altitude facility. In this paper, the authors address unsteady issues and assess the risk for facility un-start from afterburning.

Unsteady simulations were carried out to study the engine shutdown process in a simplified facility that was devoid of the turning duct. The purpose behind the simulation was to understand the physics behind the interactions

between the steam ejectors, the test cell and the supersonic diffuser. In general, it was observed that as the engine lost power, a rarefaction wave traveled downstream that disrupted the shock cell structure in the supersonic diffuser. Flow from the test cell was seen to respond by expanding into the supersonic diffuser section and re-pressurizing the area around the nozzle. An upstream traveling compression wave emanated from near the first stage ejectors due to the first stage ejector expanding to the center of the duct. However, both stage ejectors kept the facility pressurized and prevented any large amplitude pressure fluctuations from affecting the engine nozzle. Overall, the resultant nozzle pressure loads due to the nominal shutdown process were small and within the acceptable range. Of course, the pressure waves predicted during engine-shutdown were unique to this model, especially considering the fact that the turning duct was not included. The full diffuser system has been modeled, yet it's behavior is dependent on the GN2 test cell purge rate specified. Further investigation is currently planned to model the full system with the expected GN2 rates and ejector shutdown timing as completion of a Phase II SBIR program in this area.

Reacting flow simulations were also carried out in the current work to study the risk of afterburning in the facility and provide any necessary recommendations for mitigating potential problems. The numerical simulations revealed that in the case of excess unburned oxygen being emitted from the steam ejector units, there existed the possibility of afterburning inside the diffuser duct. The excess hydrogen from the engine and oxygen from the ejectors mixed in the turning duct and underwent shock-induced ignition both along the outer wall of the turning duct and at the exit of the turning duct near the second stage ejectors. As a result of the concomitant heat release, the pressure and temperature in the turning duct rose resulting in a facility un-start condition. Further simulations/investigations are underway to determine a safe threshold for oxygen concentration where the facility can operate without combustion facilitated disruption.

V. Acknowledgments

The CRAFT-Tech authors acknowledge funding for this work through a NASA SBIR, Contract Number NNX08CA36C funded by NASA Stennis Space Center. Dr Robert Field was the project monitor. We would also like to thank Mr. David Coote, Dr. Harry Ryan and Mr. Jody Woods of NASA Stennis for their recommendations and suggestions.

VI. References

1. Allgood, D., Graham, J., Ahuja, V., and Hosangadi, A., "Computational Analyses in Support of Sub-scale Diffuser Testing for the A-3 Facility - Part I: Steady Predictions", AIAA-2009-5205, 45th AIAA Join Propulsion Conference, Denver, CO, Aug. 2-5, 2009.

2. Hosangadi, A., Lee, R.A., York, B.J., Sinha, N. and Dash, S.M., "Upwind Unstructured Scheme for Three-Dimensional Combusting Flows," *Journal of Propulsion and Power*, Vol. 12, No. 3, May-June 1996, pp. 494-503.

3. Hosangadi, A., Lee, R.A., Cavallo, P.A., Sinha, N., and York, B.J., "Hybrid, Viscous, Unstructured Mesh Solver for Propulsive Applications," AIAA-98-3153, AIAA 34th JPC, Cleveland, OH, July 13-15, 1998.

4. Hosangadi, A., Cavallo, P.A., Arunajatesan, S., Ungewitter, R. and Lee, R.A., "Aero-Propulsive Jet Interaction Simulations Using Hybrid Unstructured Meshes," AIAA Paper-99-2219, 35th AIAA/ASME/SAE/ASEE Joint Propulsion Conference and Exhibit, Los Angeles, CA, June 20-24, 1999.

5. Barth, T.J., "Numerical Aspects of Computing Viscous High Reynolds Number Flows on Unstructured Meshes," AIAA Paper 91-0721, Jan. 1991.

6. Barth, T.J., and Linton, S.W., "An Unstructured Mesh Newton Solution for Compressible Fluid Flow and Its Parallel Implementation," AIAA Paper 95-0221, 1995.

7. Chidambaram, N., Kenzakowski, D.C., and Dash, S.M., "Application of Variable Turbulent Prandtl/Schmidt Methodology to Propulsive Flows," AIAA Paper No. 2000-0885, 38th AIAA Aerospace Sciences Meeting at Reno, NV, January 10-13, 2000.

8. Calhoon, W., Jr., and Kenzakowski, D.C., "Evaluation Of A PDF Turbulent-Chemistry Interaction Model For Missile Exhaust Plume Analysis," AIAA Paper No. 2000-0187, 38th AIAA Aerospace Sciences Meeting at Reno, NV, January 10-13, 2000.

9. Choi, Y-H. and Merkle, C.L., "The Application of Preconditioning to Viscous Flows," *Journal of Computational Physics*, Vol. 105, pp. 207-223 (1993).